# Magnetization and Critical Supercurrents

Y. B. Kim,* C. F. Hempstead, and A. R. Strnad

*Bell Telephone Laboratories, Murray Hill, New Jersey*

(Received 30 July 1962; revised manuscript received 5 October 1962)

The magnetization in high-field superconductors has been investigated using tubular samples. When the sample assumes a critical state, wherein every region of the sample carries critical current density $J(B)$ determined only by the local magnetic field B, the magnetization can be predicted quantitatively from the critical current density $J(B)$. Using observed magnetization data, a critical current density relation $\alpha/J = B_0 + B$ is deduced for $Nb_3Sn$ and 3Nb-Zr. $\alpha$ is a direct measure of the current carrying capacity of a sample, and $B_0$ coincides approximately with the thermodynamic critical field of the material. Since this relation implies $JB = \alpha = $ const for $B \gg B_0$, the Lorentz force plays an important role in determining the critical current density.

## I. INTRODUCTION

IN contrast to the homogeneous structure of an ideal soft superconductor, hard superconductors are often visualized as meshes of superconducting filaments surrounded by normal regions.[1] In hard superconductors, the Meissner effect is no longer complete and magnetic fields penetrate into the interior to a varying degree, yet the superconductivity persists up to a critical magnetic field $H_k$ which is often much larger than the thermodynamic critical field $H_c$. For the high-field superconducting materials[2] such as Mo-Re, Nb-Zr, and Nb-Sn, $H_k/H_c$ lies in the vicinity of thirty.[3] The magnetic properties of hard superconductors can be treated theoretically on the basis of thermodynamic energy density if one includes a surface energy term contributed by the filamentary structure. The work of Abrikosov[4] and of Goodman[5] indicates that a negative surface energy causes, under certain circumstances, a superconductor to break up into a filamentary structure and may lead to a mechanism favoring high $H_k/H_c$. Such theories, however, generally predict a size independent magnetization and do not explain the size-dependent magnetization commonly observed in hard superconducting materials.[6,7] Bean,[7] on the other hand, treats the magnetization as resulting directly from the supercurrents generated in a sample and regards the critical current carried by the filaments as the prime factor in determining the magnetization. As the total critical current carried by all the filaments is proportional to the size of a sample, Bean's treatment leads directly to a size-dependent magnetization. Since the magnetic properties of a superconductor are believed to originate from the supercurrents in the sample,

Bean's approach is more direct from the phenomenological point of view. If successful, it is also more economical in that the fundamental theory needs to explain only one set of data, i.e., the critical current density.

In the present work we generalize Bean's approach and introduce the concept of *critical states*, wherein every macroscopic region of a sample carries a maximum supercurrent (critical current) determined only by the local magnetic field at that region. This assumption of a unique critical current for a given field makes the analytical treatment of the problem quite definitive. On the experimental side, the use of thin-walled tubular samples, instead of solid cylindrical specimens, allows more sensitive testing of predictions of the theory. No specific assumption is made regarding the microstructure of the sample in a critical state, but a mechanism leading to the critical state is envisioned as follows.[7] If the externally applied magnetic field (directed along the tube axis) is increased, for example, currents are induced in the sample which counteract the change in the external field. Initially, the induced currents may be confined on the sample surface. As the field is further increased, however, the induced currents progressively spread into the interior of the sample, eventually reaching a critical state as described above. In general, the critical current density of a hard superconductor decreases as the applied field increases. Thus, once the critical state is reached, a further increase in the external field tends to reduce the critical currents in the sample since the mean field in the sample becomes larger.

The experimental results presented in this paper can be satisfactorily explained in terms of the critical states as defined above. More refined measurements, however, reveal that the critical states which were initially thought to be sharp boundaries between superconducting and normal states, are only quasi-equilibrium states and the critical currents generated in a sample decay slowly. This observation injects new features into the problem of hard superconductors.[8,9]

* On leave of absence from University of Washington, Seattle, Washington.

[1] This picture was first suggested by K. Mendelssohn, Proc. Roy. Soc. (London) **A152**, 34 (1935).

[2] J. E. Kunzler, Rev. Mod. Phys. **33**, 1 (1961).

[3] R. D. Blaugher and J. K. Hulm, Phys. Rev. **125**, 474 (1962).

[4] A. A. Abrikosov, J. Exptl. Theoret. Phys. (U.S.S.R.) **32**, 1442 (1957) [translation: Soviet Phys.—JETP **5**, 1174 (1957)].

[5] B. B. Goodman, Phys. Rev. Letters **6**, 597 (1961).

[6] F. J. Morin, J. P. Maita, H. J. Williams, R. C. Sherwood, J. H. Wernick, and J. E. Kunzler, Phys. Rev. Letters **8**, 275 (1962).

[7] C. P. Bean, Phys. Rev. Letters **8**, 250 (1962).

[8] Y. B. Kim, C. F. Hempstead, and A. R. Strnad, Phys. Rev. Letters **9**, 306 (1962).

[9] P. W. Anderson, Phys. Rev. Letters **9**, 309 (1962).

Nevertheless, within a laboratory time scale, the reduction of critical currents due to this decay amounts to only a few tenths of a percent of the initial level. Thus, the relation between the magnetization and the critical current, the subject matter of the present paper, is not modified substantially by this decay process.

## II. EXPERIMENTAL

In the present experiments, the magnetization of high-field superconducting material (Nb-Zr, Nb-Sn) is measured using tubular samples. In this method, a uniform external magnetic field $H$ is applied in the direction of the tube axis and the field $H'$ at the tube center is measured using a sensitive magnetoresistance probe.[10] The difference $M = H' - H$ is attributed to the supercurrents induced in the tube.

A typical $H'$ vs $H$ curve obtained by this method is shown in Fig. 1. As $H$ is slowly increased from zero, $H'$ remains at zero until $H$ reaches point (1). Part or all of the tube then suddenly becomes normal, the flux breaks into the interior of the tube, and we say that a "flux jump" has taken place. After such a flux jump occurs, $H$ is held constant for several minutes to allow the sample to reach thermal equilibrium with its surroundings. As $H$ is further increased, the tube again shields the external field until it undergoes another flux jump at point (2). At points (1) and (2), the tube carried supercurrents corresponding to $M = -15$ kG, and $-25$ kG, respectively. Since hard superconductors generally are capable of carrying more current at lower fields, one may infer that at point (1) the tube did not attain the maximum current which the sample could carry under proper conditions at that given field. That is, it did not attain a critical state. In
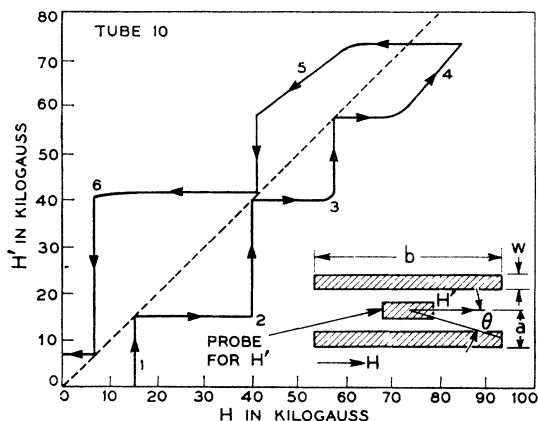


Fig. 1. Magnetization of a tube sample. $H'$ is the magnetic field measured inside the tube, and $H$ the external magnetic field applied parallel to the tube axis.

10 The magnetoresistance probe used in the present experiment was wound noninductively with 5 mil pure copper wire (purity 0.9999). For magnetic fields higher than a few kilogauss, the probe resistance increases linearly with the field and probe resolution is good to 10 G. We are indebted to J. E. Kunzler for suggesting the use of magnetoresistance probes.
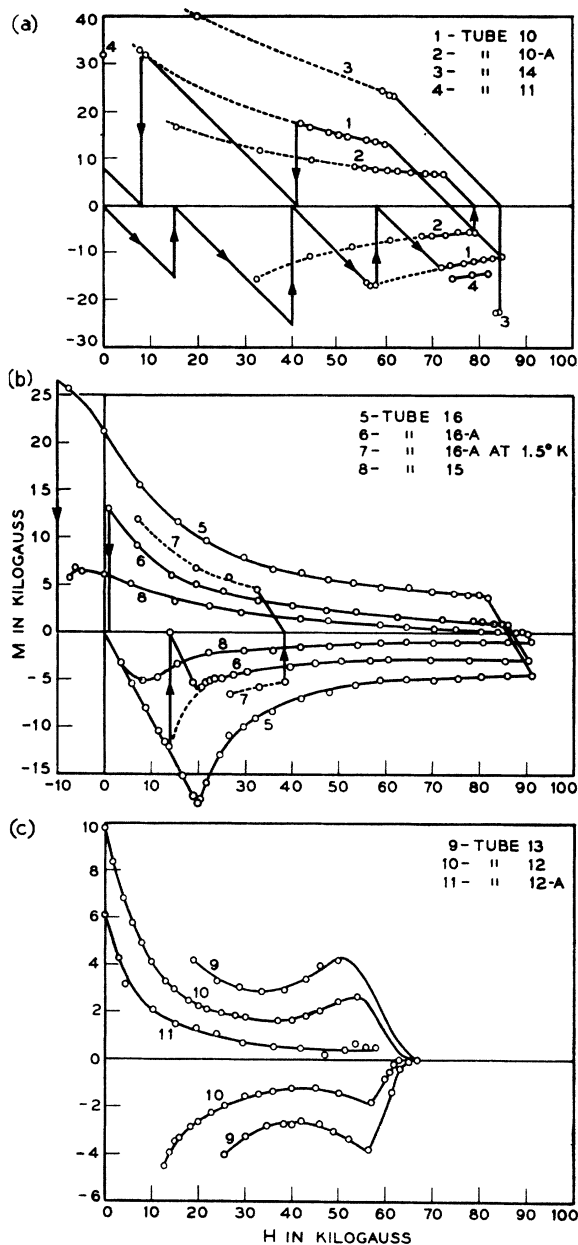


Fig. 2. $M = H' - H$ vs $H$ for various tube samples. Unless specified otherwise, all runs were taken at $T = 4.2°$K.

region (3), however, $H'$ begins to increase gradually with $H$ before it undergoes a flux jump. This behavior we take to be the indication that the tube is beginning to assume critical states. Once the high-field region (4) is reached, the tube continues to be in critical states. For decreasing $H$, the tube attains critical states in region (5) and at point (6).

Inasmuch as $M$ is a direct measure of the total current induced in the tube, it is revealing to plot $M$ vs $H$. Such plots obtained for various $Nb_3Sn$ sintered samples are shown in Figs. 2(a) and 2(b). For samples carrying small currents [Fig. 2(b)], the critical state

TABLE I. Descriptions of tube samples.

| Material | Tube No. | Sintering | Density (g/cm³) | Geometry a (cm) | Geometry w (cm) | Geometry θ (deg) | J* (10³ A/cm²) at H* 30 (kG) | 50 (kG) | 70 (kG) | $H_s$ (kG) | $H_s'$ (kG) | α (10⁶ kG-A/cm²) | $B_0$ (kG) |
|---|---|---|---|---|---|---|---|---|---|---|---|---|---|
|  | 10 | 2 h–1000°C | 7.5 | 0.419 | 0.121 | 18.0 | 190 | 120 | 87 | ... | ... | 6.5 | 4.5 |
|  | 10-A | 2 h–1000°C | 7.5 | 0.419 | 0.062 | 19.3 | 190 | 120 | 88 | ... | ... | 6.5 | 4.8 |
|  | 14 | 2 h–985°C | 6.5 | 0.426 | 0.245 | 15.8 | ... | 110 | 82 | ... | ... | 6.6 | 7.4 |
| Nb₃Sn | 11 | 2 h–1100°C | 7.5 | 0.419 | 0.241 | 15.1 | ... | ... | 52 | ... | ... | ... | ... |
|  | 16 | 4 h–1200°C | 5.9 | 0.405 | 0.226 | 26.0 | 34 | 22 | 18 | 20.0 | 21.2 | 1.2 | 5.0 |
|  | 16-A | 4 h–1200°C | 5.9 | 0.405 | 0.113 | 30.2 | 32 | 22 | 17 | 14.0 | 13.5 | 1.1 | 3.7 |
|  | 16-A (1.5°K) | 4 h–1200°C | 5.9 | 0.405 | 0.113 | 30.2 | 46 | ... | ... | ... | ... | 1.6 | 4.0 |
|  | 15 | 4 h–less than 985°C | 6.5 | 0.405 | 0.225 | 25.7 | 8.0 | 5.0 | 2.8 | 5–8 | 6.1 | 0.28 | 5.0 |
|  | "wire" | 16 h–1000°C | 7.5 | 0.25 cm diameter | | | 210 | 135 | 97 | ... | ... | 7.5 | 6.0 |
| Nb | 13 | ... | 7.9 | 0.945 | 0.762 | 12.5 | 3.3 | 3.8 | ... | ... | ... | 0.11 | 1.9 |
| 25 at.% | 12 | ... | 7.9 | 0.564 | 0.381 | 8.2 | 3.6 | 4.0 | ... | 9.5 | 9.9 | 0.11 | 0.6 |
| Zr | 12-A | Annealed 1 h–1125°C | 7.9 | 0.564 | 0.381 | 16.0 | 1.7 | 0.9 | ... | ... | ... | 0.056 | 0.8 |

region is obtained for the whole range of $H$ available. For samples capable of carrying large currents [Fig. 2(a)], however, flux jumps take place frequently. The history of flux jumps is shown for only one sample (tube 10). For all the other samples, solid lines indicate continuous regions of critical states, and dashed lines are drawn through isolated critical state points observed.

For a given $H$, the magnitude of field *shielding* current corresponding to negative $M$, $(M_- = H - H')$, is usually larger than the field *trapping* current corresponding to positive $M$, $(M_+ = H' - H)$. Such a disparity between $M_+$ and $M_-$ is expected since, the external field $H$ being the same, the tube "sees" effectively a larger average field under $M_+$ condition than under $M_-$ condition. This disparity can be removed to a certain extent by comparing $M$'s at

$$H^* = \tfrac{1}{2}(H' + H) = H + M/2 = H \pm M_\pm/2 \qquad (1)$$

$M_\pm$'s plotted vs the mean field $H^*$ are shown in Fig. 3. The disparity is reduced but still exists, particularly for low critical currents at high fields. Without attaching too much significance to this disparity, we tentatively deduce the critical current density from the relation

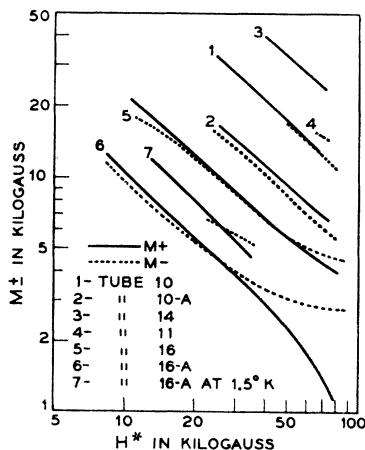$$\langle M \rangle = \tfrac{1}{2}(M_+ + M_-) = kwJ^* \cos\theta, \qquad (2)$$



FIG. 3. $M_+$ and $M_-$ vs $H^*$. $H^* = (H+H')/2$ is the mean magnetic field in the sample.

where $w$ is the wall thickness in cm, $\theta$ the opening angle of the tube (see Fig. 1), and $k = 0.4\pi$ G-cm/A. The assumptions leading to Eq. (2) are discussed in Sec. III. Although actual distributions of field and current density in the samples are not known, the present experiment yields their effective mean values, $H^*$ and $J^*$.

The critical current densities obtained in this manner are listed in Table I, together with other pertinent data. For Nb₃Sn samples sintered under similar conditions, the current densities are practically independent of wall thickness, or the current is proportional to the cross sectional area of a sample. This behavior has also been observed in Nb₃Sn "wire" samples,[2] and indicates that no macroscopic Meissner effect is operating. For tubes 10, 10-A, and 14, the magnitudes of current densities compare favorably with that of a typical "wire" sample. If the high current capacity of hard superconductors is attributed to strains and inhomogeneities in the material, then in Nb₃Sn such a state appears to set in during the sintering process. Varying critical current densities observed for different groups of Nb₃Sn samples are probably caused by differences in sintering temperatures and times.[11]

$M$ vs $H$ plots obtained for 3Nb-Zr alloy tubes are shown in Fig. 2(c). Here again we find that the critical current densities are independent of wall thickness. However, for the bulk samples we used the magnitude of current density is less by a factor 10 than that obtainable with wire samples of much smaller cross sectional area. Thus, in Nb-Zr material cold work applied during the wire drawing process appears to increase current capacity significantly. The so-called "peak" effect,[12] which is commonly observed with rolled Nb-Zr samples and is attributed to anisotropy in the material, is present also in our bulk samples. For an annealed

[11] More systematic studies on the effect of sintering temperatures and times have been carried out by R. E. Enstrom, G. W. Pearsall, and J. Wulff, Bull. Am. Phys. Soc. 7, 323 (1962); E. Buehler, J. H. Wernick, K. M. Olsen, F. S. L. Hsu, and J. E. Kunzler (to be published).

[12] The peak effect in Nb-Zr alloys was first observed by T. G. Berlincourt, R. R. Hake, and D. H. Leslie, Phys. Rev. Letters 6, 671 (1961).

bulk sample (tube 12-A), the critical current is less and the peak effect seems to disappear.

We now wish to comment on the phenomenon of flux jumps. In general, flux jumps occur less frequently when the external field is changed slowly with small fluctuations.[13] In most of our runs, we varied the external field as slowly as was practical. However, for a given rate of external field change we have found that critical states become increasingly difficult to realize as $|M|$ increases. For example, in tube 16-A the continuous critical state region was obtained at 4.2°K. At 1.5°K, $|M|$ increased because of the increase in critical current density, but critical states were possible only at isolated points. On the other hand, in tubes 10-A, 10, and 14 critical states are more difficult to realize for thicker wall tubing carrying larger currents, yet for a given $H^*$ they all carry about the same average current density. It thus appears that the instability leading to flux jumps is associated with a large $|M|$, but not necessarily with a large critical current density. We note also that for a given $|M|$, flux jumps set in more often at $M_-$ condition where the internal field $H'$ is varying rapidly relative to the external field $H$. On the basis of critical current density alone, a $Nb_3Sn$ tube of 1-cm wall could trap a field close to 100 kG, but the aforementioned instability prevents this. The best we were able to achieve in the present experiment was a 32 kG genuine trapping (zero external field) in tube 11. Tube 14 carried a current corresponding to 40 kG at $H=20$ kG and $H' = 60$ kG, but it went normal soon after.

### III. ANALYSIS

#### A. Magnetization at Critical States

In the previous section we used the term "critical state" rather loosely to describe a superconducting state in which the sample as a whole attains a critical current. However, the experimental observations indicate strongly that the critical current attained by a sample in such a state is a body current in saturation and the concept of critical current may apply to every region of the sample. We, therefore, formally postulate the existence of critical states as defined in Sec. I. When a superconducting sample is in such a state at a given temperature and pressure, *every macroscopic region* of the sample carries a critical current density $J(B)$ determined only by the local magnetic field $B$ at that region. This assumption of a unique $J(B)$ for a given $B$ enables us to determine the state of magnetization completely through the relations

$$B = H + 4\pi m,$$
$$J(B) = c\nabla \times m, \qquad (3)$$

once the external field $H$ and its history are specified.

[13] Similar behavior was observed in $Nb_3Sn$ tubes by F. Rothwarf, R. C. Thiel, S. H. Autler, and K. Gooen, Bull. Am. Phys. Soc. 7, 189 (1962).
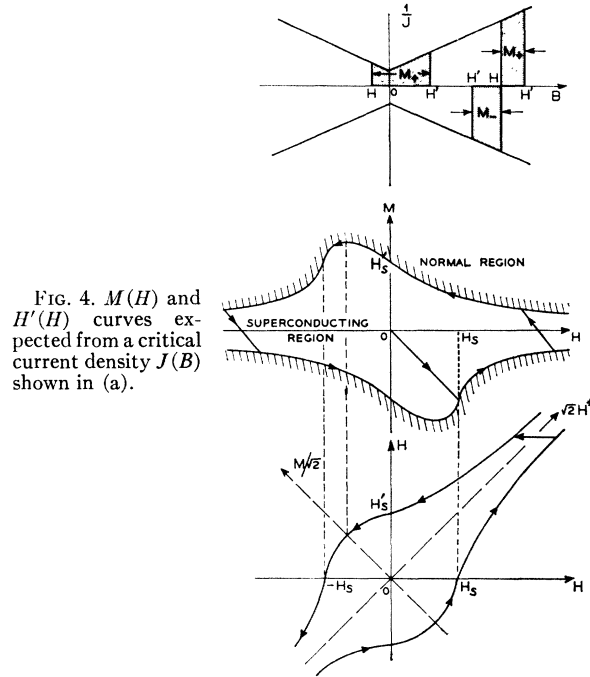


FIG. 4. $M(H)$ and $H'(H)$ curves expected from a critical current density $J(B)$ shown in (a).

When the history of the external field is repeated, we therefore expect a magnetization curve comprised of critical states to be retraceable within the slight fuzziness caused by the slow decay of $J(B)$. For an infinitely long cylinder of outer radius $a$, to which a uniform external field $H$ is applied parallel to the axis, (3) reduces to a scalar equation

$$B(r) = H + m(r) = H + k \int_r^a J[B(x)]dx, \qquad (4)$$

where $x$ and $r$ are radial variables in cm, and $k = 0.4\pi$ G-cm/A as in the previous section.

While (4) is useful in describing the distributions of currents and fields in the sample, the state of magnetization can be discussed more conveniently in terms of an integral relation

$$k(a-r) = \int_H^{H+m(r)} \frac{dB}{J(B)}. \qquad (5)$$

Both $J$ and $m$ are negative for increasing $H$ and positive for decreasing $H$. The magnitude of $J$ is determined only by the absolute value of $B$. The origin of (5) is clear since it reduces to $m = Jk(a-r)$ when $a-r$ is infinitesimally small.

We now apply (5) for tubular samples. For a tube of wall thickness $w$, we measure the field $H' = B(r = a-w)$ and obtain $M = m(r = a-w) = H' - H$. $M$ so derived is a direct measure of the total current in the tube and can be represented as a function of either $H$ or $H^* = H + (M/2)$, the mean field in the sample. The latter
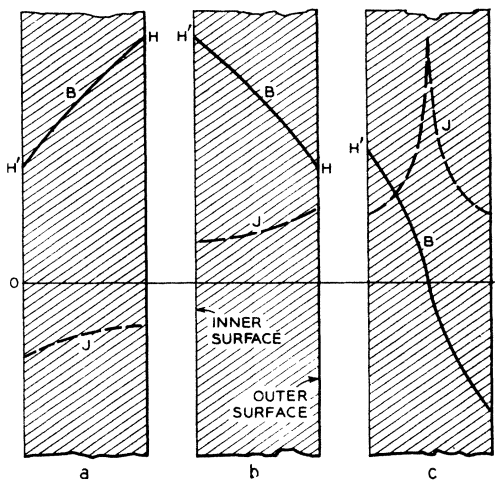
Fig. 5. The distribution of $B$ and $J$ in the sample
for three typical cases.

representation is more appropriate when we talk about the average current density $J^*(H^*)=M(H^*)/kw$. In a critical state these experimental quantities are determined by $J(B)$ through

$$kw=\int_H^{H'}\frac{dB}{J(B)}=\int_H^{H+M}\frac{dB}{J(B)}=\int_{H^*-M/2}^{H^*+M/2}\frac{dB}{J(B)}. \quad (6)$$

In Fig. 4 we show graphically how this relation is used to derive the magnetization curve. We assume here that $1/J(B)$ is linear in $B$. Such a distribution is shown to be reasonable from our experimental data. The set of all critical states forms the boundary between the superconducting and normal regions, and (6) is applicable only for the points on this boundary.[14] As $H$ is increased from zero, $M$ follows the 45° line giving $M=-H$. But the sample does not attain a critical state until $H$ reaches $H_s$, where the field begins to penetrate into the interior of the tube. From this point on $M$ follows the boundary line. For decreasing $H$, $M$ passes through noncritical states before it reaches the boundary line at the positive side. When $H$ is reduced to zero, the tube is left with a trapped field $H_s'$. The distributions of magnetic fields and currents in the sample are shown in Fig. 5 for three representative cases.

The following general features of the magnetization curve can be derived from (6) without specifying the form of $J(B)$.

(i) Since (6) is invariant under the transformation $(H,H')\to(H',H)$, the $H'(H)$ curve is symmetric with respect to the 45° line. We shall call this symmetry the folding symmetry. The $H'(H)$ curve is also expected to have a reflection symmetry on general

---

[14] In view of the slow decay of critical currents, however, the region we designated as superconducting is partially normal, particularly near the boundary curves. This decay process also makes the boundary curve itself somewhat fuzzy.

grounds. In the present cylindrical geometry, this follows from the invariance of (6) under the transformation $(H,H')\to(-H,-H')$.

(ii) A specific prediction resulting from the folding symmetry is that $H_s=H_s'$.

(iii) For a given $H(>H_s)$, the magnitudes of the two $M$ values, $M_+(H)$ and $M_-(H)$, are different in general. This disparity between $M_+(H)$ and $M_-(H)$ is governed by the first derivative of $J(B)$, i.e.,

$$M_+(H)\underset{>}{\overset{<}{\geqslant}}M_-(H) \quad\text{if}\quad \frac{d}{dB}\frac{1}{J}\underset{<}{\overset{>}{\gtrless}}0.$$

(iv) This disparity is removed in the $H^*$ representation, i.e., $M_+(H^*)=M_-(H^*)$. This follows from the fact that the third expression of (6) is invariant under the transformation $(M,J)\to(-M,-J)$, and is a consequence of the folding symmetry.

(v) The proximity of $J^*(H^*)$ to $J(H^*)$ is governed by the second derivative of $J$, i.e.,

$$J^*/J\underset{>}{\overset{<}{\geqslant}}1 \quad\text{if}\quad \frac{d^2}{dB^2}\frac{1}{J}\underset{<}{\overset{>}{\gtrless}}0.$$

If $1/J$ is a linear function of $B$, $J^*=J$ is a precise statement. When $1/J$ deviates from this linearity, $J^*$ moves away from $J$ in such a direction as to accentuate the corresponding nonlinearity in $1/J^*$.

(vi) In a converse situation where we are given $M(H^*)$ from the experiments, the above relation holds in a diluted form:

$$\int_{H^*-M/2}^{H^*+M/2}\left(\frac{1}{J}-\frac{1}{J^*}\right)dB\underset{>}{\overset{<}{\geqslant}}0 \quad\text{if}\quad \frac{d^2}{dH^{*2}}\frac{1}{M}\underset{<}{\overset{>}{\gtrless}}0.$$

(vii) If $M\ll H^*$, then $J^*\simeq J$ independent of their forms. This approximate identity also holds for the first derivatives of $\log J^*$ and $\log J$.

These results, obtained thus far without assuming a specific form of $J(B)$, are compared with our experiments. The observed values of $H_s$ and $H_s'$ listed in Table I verify that $H_s=H_s'$. We observe $M_-(H)>M_+(H)$ in most cases, indicating that $J(B)$ is a decreasing function of $B$ in most regions. When $M$ is plotted vs the mean field $H^*$, the disparity is reduced but still exists, particularly in the region of small $|M|$ and large $H^*$ (Fig. 3). In view of (iv), this observed disparity should be attributed to the end effects arising from the finite tube lengths. Although we observed a shorter tube to give a more pronounced disparity, this question should be answered by additional experiments, or by solving (3) in its full generality. In spite of this disparity, however, it is found that $\log M$ vs $\log H^*$ plots (Fig. 3) for various $Nb_3Sn$ samples contain straight line regions of slope close to $-1$. This behavior is also noted for 3Nb-Zr tubes for $H^*$ up to about 35 kG. On the strength of (v) and (vi), we then conclude that $J^*$ obtained in our tube experiments is probably a correct

representation of $J$ and $1/J$ is linear in $B$. It is, therefore, worthwhile to explore the consequence of this specific distribution.

We now take a distribution

$$\alpha/J = B_0 + B, \tag{7}$$

involving two constants $\alpha$ and $B_0$. Substitution of (7) into (6) yields

$$\alpha k w/M(H^*) = B_0 + H^*, \tag{8}$$

indicating that the two constants $\alpha$ and $B_0$ can be determined from the experiments. Solving (6) in $H'$ and $H$ with the notations

$$H/B_0 = h, \quad H'/B_0 = h', \quad A = 2\alpha k w/B_0^2, \tag{9}$$

we obtain hyperbolas

$$(h'+1)^2 - (h+1)^2 = \pm A. \tag{10}$$

The $-$ sign is to be used for $H > H' > 0$ and $+$ sign for $H' > H > 0$. For $H < 0 < H'$, we obtain a circle

$$(h'+1)^2 + (1-h)^2 = A + 2. \tag{11}$$

$M(H)$'s corresponding to (10) and (11) are given by

$$M/B_0 = \{(h+1)^2 \pm A\}^{1/2} - (h+1), \tag{10'}$$

$$M/B_0 = \{A + 2 - (1-h)^2\}^{1/2} - (h+1). \tag{11'}$$

Equation (10) or (10') predicts

$$H_s/B_0 = H_s'/B_0 = (1+A)^{1/2} - 1. \tag{12}$$

Thus, $H_s$ is proportional to $w$ for $A \ll 1$, while it is proportional to $\sqrt{w}$ for $A \gg 1$.

The magnetization curve resulting from (10') and (11') for $B_0 = 5$ kG and $A = 25$ is shown as solid lines in Fig. 6. These particular values for $B_0$ and $A$ were chosen from the plot of (8) for tube 16. While the general fit of experimental points to the calculated curve is expected from (8), the specific agreement in
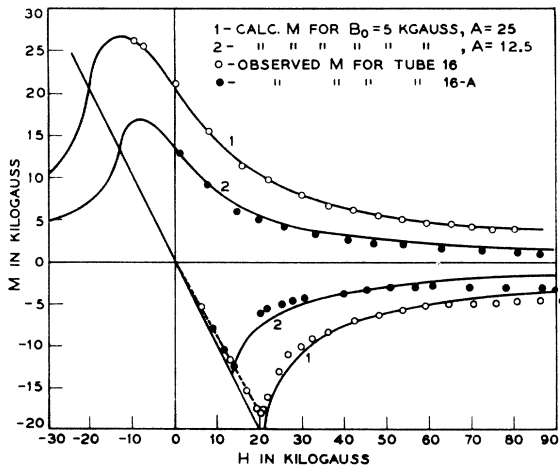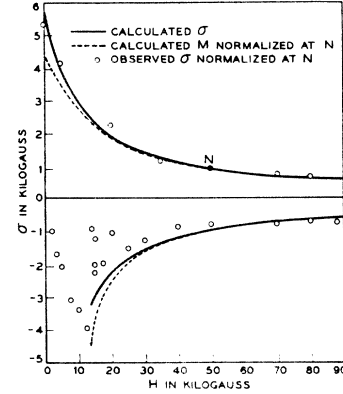


Fig. 6. $M(H)$ curves calculated from the theory compared with the experimental data.



Fig. 7. Magnetization for a solid cylinder calculated from the theory and the experimental data for $V_3$Ga sample given in reference 6.

the $H_s$ value and the fit of experimental points to (11') enhances our confidence in the present theory. Furthermore, the calculated curve for $B_0 = 5$ kG and $A = 12.5$, corresponding to the same material but with the wall thickness reduced by one-half, traces very well the data points for tube 16-A. The experimental data for tube 16-A, which are shown in the figure without any normalization, were taken after reducing the wall thickness of tube 16 by one-half.

We now consider the magnetization of a long solid cylinder. For such a sample, one measures experimentally the spatial average of $m(r)$:

$$\sigma = \frac{1}{\pi a^2} \int_0^a 2\pi r m(r) dr. \tag{13}$$

Clearly, other conditions being the same, the tube experiment which measures $m(r)$ at one point is more sensitive in reflecting $J(B)$ since it involves one less integration. For the distribution given by (7), we obtain

$$\sigma = M(8\nu^2 + 25\nu + 20)/15(2+\nu)^2; \quad \nu = M/(B_0 + H), \tag{14}$$

where $M = m(r=0)$ is to be obtained from (10') by replacing $w$ with $a$. The values of $\sigma$ calculated from (14) with $B_0 = 5$ kG and $A = 12.5$ are shown in Fig. 7 by the solid line. For a given external field $H$, $|M|$ is always larger than $|\sigma|$. However, to indicate their relative shapes, $M$ curves have been normalized at $\sigma_+$ for $H = 50$ kG. At low fields where $|M|$ is large, $\sigma_\pm$ deviates considerably from $M_\pm$. This behavior comes from the fact that $\sigma$ weighs more heavily the current distribution toward the outer wall, which is large for $M_+$ and small for $M_-$. The experimental data on $V_3$Ga obtained by Morin et al,[6] are shown in the figure with one point normalization. The close fit of experimental points to the calculated curve may be somewhat fortuitous. However, it indicates that if two parameters $B_0$ and $A$ appearing in the present theory are properly adjusted, the theory is capable of predicting the observed magnetization curve. The scattering of $\sigma_-$ points observed at low fields is reminiscent of the difficulty of obtaining critical states in the tube
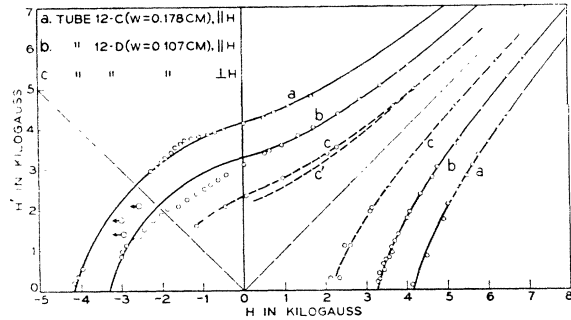
FIG. 8. $H'(H)$ for 3Nb-Zr tubes of two different wall thickness. Open circles with arrows indicate the points where the sample went normal before reaching critical states. (c') is the folding symmetry of (c) below the 45° line.

experiment. $\sigma_-$ for small $H$ is not given in the present theory since the sample does not assume critical states in this region. Bean[7] derives the magnetization in this region using (7) in a simplified form $J = \text{const}$.

The existence of critical states is basic to the present theory and it can be tested experimentally from the retraceability of the magnetization curve. The theory then predicts a definite symmetry in $H'(H)$ independent of the form of $J(B)$. The experiments described in Sec. II were not adequate to test these basic points. In fact, the present theory began to take its shape only after we represented our data in the form of Fig. 3. We, therefore, performed additional experiments at low fields using a 3Nb-Zr tube of two different wall thickness. The data obtained from several different runs are shown together in Fig. 8 to demonstrate the retraceability of critical states. The data points obtained in third and fourth quadrants are transferred to the first and second quadrants to demonstrate the reflection symmetry. The folding symmetry is also evident from the data. For each set of data $\alpha$ and $B_0$ are obtained from (8), and two hyperbolas and one circle predicted by (10) and (11) are shown by the solid lines. In the circular regions the data points deviate from the predicted curves, particularly for tube 12-D. When the external field is reduced to zero, the outer surface of the tube is in a zero field condition. As $H$ continues to decrease (in the negative direction), the zero field point moves into the sample (see Fig. 5). Thus, in the circular region, a substantial portion of the sample "sees" magnetic field less than the thermodynamic critical field and the possibility of Meissner currents cannot be ruled out. In fact, in this region $H$ often undergoes a stepwise variation, of the order of 50 G. Flux jumps are difficult to avoid near the 135° line, where $M$, and hence the total current in the sample, is maximum. This instability is discussed shortly. Data points taken with the external field transverse to the tube axis are shown for tube 12-D. Both the retraceability and the reflection symmetry hold here, but the folding symmetry no longer exists. The distributions of current and fields are rather complex in this case

and no attempt has been made to fit the data with calculations.

## B. Flux Jump

In the present experiment, the current in a superconductor is generated by a time-dependent magnetic field according to the law of induction

$$\nabla \times \mathbf{E} = - (1/c)(\partial \mathbf{B}/\partial t) \tag{15}$$

For our cylindrical geometry, this reduces to a scalar equation

$$E = - (1/c2\pi r)[d\varphi(r,t)/dt], \tag{16}$$

where

$$\varphi(r,t) = \int_0^r B(x,t)2\pi x\,dx \tag{17}$$

is the flux contained in a cylinder of radius $r$. So far we have considered only an adiabatic change in $B$, so that $E \simeq 0$ and only the Lenz's law part of (15) comes into the analysis. When $dB/dt$ is appreciable, however, the resulting electric field $E$ may also generate a normal current

$$J_n = E/\rho = - (1/c\rho 2\pi r)(d\varphi/dt). \tag{18}$$

As long as the supercurrent $J_s$ is capable of following the change in magnetic field by the acceleration mechanism

$$dJ_s/dt = (c^2/4\pi\lambda^2)E, \tag{19}$$

the effect of $J_n$ is expected to be completely negligible. For ordinary soft superconductors, numerical values of the penetration depth $\lambda$ and the resistivity $\rho$ for the normal electrons are such that $J_n$ becomes significant only for rapidly varying fields in the hundred megacycle range.[15] For high-field superconductors such numerics may not hold, but we do not detect experimentally any evidence for $J_n$ in the noncritical state. Once a critical state is reached, however, $J_s$ no longer follows (19) and the generation of $J_n$ cannot be suppressed. In this situation, any fast change in magnetic field tends to heat up the sample and may induce a sudden transition to a normal state, or a flux jump.

To analyze this transient behavior qualitatively, we consider the total normal current $i_n$ and associate with it effective inductance $L$ and resistance $R$. (18) is then reducible to an ordinary circuit equation,

$$(d/dt)(Li_n + \psi) = Ri_n, \tag{20}$$

where $\psi$ is the "external" flux linkage seen by the normal current $i_n$. $\psi$ consists of the flux linkages due to the external field $H$ and the supercurrent $i_s$. We now suppose that $\psi$ is changed from $\psi_1$ to $\psi_2$ uniformly over a period $T$. In this case $i_n$ builds up to a maximum value at $t = T$ and gradually decays, thereafter, with a time constant $\tau = L/R$. The total heat energy gen-

[15] D. Shoenberg, *Superconductivity* (Cambridge University Press, New York, 1960).

erated by $i_n$ is then given by

$$W = [(\psi_1 - \psi_2)^2/L]f(T/\tau) \qquad (21)$$

where $f = 1/2$ for $T/\tau = 0$ and decreases monotonically to zero for large $T/\tau$. Thus, the heating by the normal current can be reduced by changing $\psi$ slowly compared with the time constant $\tau$. For a thin wall tube of radius $a$, $\psi$ is given approximately by

$$\psi = \pi a^2 H' = \pi a^2(H+M), \qquad (22)$$

and

$$\Delta\psi = \psi_2 - \psi_1 = \pi a^2 \Delta H' = \pi a^2(\Delta H + \Delta M). \qquad (23)$$

Thus, for a given external field change $\Delta H$ with a given rate of change $\Delta H/T$,

$$W \propto (dH'/dH)^2 = (1 + dM/dH)^2, \qquad (24)$$

indicating that the heat generation is more severe in the region where the magnetization curve $H'(H)$ has a steep slope. This is in agreement with the experimental observation that the critical states are more difficult to realize when the slope of the magnetization curve is steep.

According to the above picture, a transition from one critical state to another is very difficult unless the heat generated by normal current is efficiently conducted away. If this conduction process is not fast enough, the rise in temperature begins to quench a part of the supercurrent, thereby generating more heat. Since this additional heat is proportional to $M^2$, one would expect that flux jumps are more frequent when $M$ is large. This argument clearly points out the difficulty of realizing a critical state for a bulk superconductor of large size.

*Note added in proof.* Recently, three Nb$_3$Sn tubes each shielded more than 30 kG (one up to 40 kG) in an external field supplied by a Nb-Zr wire-wound superconducting solenoid capable of 55 kG. The rate of change of applied external field was about 10 G per sec. We have not yet determined the factor by which this rate can be increased without causing flux jumps.

Since the slow decay of critical current near a critical state also dissipates power, this effect must be included in a refined analysis of the flux jump phenomenon.

## IV. DISCUSSION

In the present investigation we have shown that the critical state magnetization in high-field superconduc-

tors can be derived quantitatively from the critical current density. More interesting is the fact that the magnetization data, in turn, can be used effectively in deducing the critical current density. While the deduction requires a somewhat involved analysis, this method automatically takes into account the nonuniform magnetic field present in a sample. The use of tubes also avoids the contact heating problem generally encountered in the conventional resistance method, and enables us to investigate the critical state conditions more leisurely.

The magnetization data obtained in the present experiment can be adequately explained in terms of a critical current density given by (7). For 3Nb-Zr samples the peak effect sets in at $B \sim 35$ kG and (7) is no longer adequate. For Nb$_3$Sn samples (7) holds up to $B \sim 70$ kG. Nb$_3$Sn samples of low critical current density, however, exhibit a marked deviation from (7) at high fields. How much of this deviation is due to the end effect is not clear at the moment. In any case, (7) is not expected to hold indefinitely since it implies infinitely large critical field $H_k$. Using the region where (7) holds the values of two constants $\alpha$ and $B_0$ are calculated (Table 1). $\alpha$ reflects directly the current carrying capacity of a sample, and varies considerably depending on how the samples are prepared. $B_0$, on the other hand, has no strong correlation to the current carrying capacity. For Nb$_3$Sn samples $B_0$ lies in the range of 4 to 7 kG, whereas it lies in the range of 1 to 2 kG for 3Nb-Zr samples.

The critical current density (7) derived in the present experiment implies $JB = \alpha$ for $B \gg B_0$. That is, the Lorentz force plays an important role in determining the critical current density. This fact, together with the strong temperature dependence of $\alpha$ and the observation of slow decay in critical currents[8] lead Anderson[9] to propose a theory of "flux creep" for hard superconductors. A detailed account of the experimental results related to this more fundamental question will be communicated in the near future.

FIG. 4. $M(H)$ and $H'(H)$ curves expected from a critical current density $J(B)$ shown in (a).